

## HD 119130 b is not an “ultra-dense” sub-Neptune

JOSEPH M. AKANA MURPHY <sup>1,\*</sup> RAFAEL LUQUE <sup>2,†</sup> NATALIE M. BATALHA <sup>1</sup> ILARIA CARLEO <sup>3,4</sup>  
ENRIC PALLE <sup>3,4</sup> MADISON BRADY <sup>5</sup> BENJAMIN FULTON <sup>6</sup> LUKE B. HANDLEY <sup>7</sup> HOWARD ISAACSON <sup>8</sup>  
GAIA LACEDELLI <sup>3</sup> FELIPE MURRAS <sup>3,4</sup> GRZEGORZ NOWAK <sup>9,3,4</sup> J. ORELL-MIQUEL <sup>3,4</sup>  
HANNAH L. M. OSBORNE <sup>10,11</sup> VINCENT VAN EYLEN <sup>10</sup> AND MARÍA ROSA ZAPATERO OSORIO <sup>12</sup>

<sup>1</sup>*Department of Astronomy and Astrophysics, University of California, Santa Cruz, CA 95064, USA*

<sup>2</sup>*Department of Astronomy and Astrophysics, University of Chicago, Chicago, IL 60637, USA*

<sup>3</sup>*Instituto de Astrofísica de Canarias (IAC), 38205 La Laguna, Tenerife, Spain*

<sup>4</sup>*Departamento de Astrofísica, Universidad de La Laguna (ULL), 38206 La Laguna, Tenerife, Spain*

<sup>5</sup>*Department of Astronomy & Astrophysics, University of Chicago, Chicago, IL 60637, USA*

<sup>6</sup>*NASA Exoplanet Science Institute/Caltech-IPAC, Pasadena, CA 91125, USA*

<sup>7</sup>*Department of Astronomy, California Institute of Technology, Pasadena, CA 91125, USA*

<sup>8</sup>*501 Campbell Hall, University of California at Berkeley, Berkeley, CA 94720, USA*

<sup>9</sup>*Institute of Astronomy, Faculty of Physics, Astronomy and Informatics, Nicolaus Copernicus University, Grudziądzka 5, 87-100 Toruń, Poland*

<sup>10</sup>*Mullard Space Science Laboratory, University College London, Surrey, UK*

<sup>11</sup>*European Southern Observatory, Karl-Schwarzschild-Straße 2, Garching bei München, Germany*

<sup>12</sup>*Centro de Astrobiología (CSIC-INTA), Crta. Ajalvir km 4, E-28850 Torrejón de Ardoz, Madrid, Spain*

### ABSTRACT

We present a revised mass measurement for HD 119130 b (aka K2-292 b), a transiting planet ( $P = 17$  days,  $R_p = 2.63_{-0.10}^{+0.11} R_\oplus$ ) orbiting a chromospherically inactive G dwarf, previously thought to be one of the densest sub-Neptunes known. Our follow-up Doppler observations with HARPS, HARPS-N, and HIRES reveal that HD 119130 b is, in fact, nearly one-third as massive as originally suggested by its initial confirmation paper. Our revised analysis finds  $M_p = 8.8 \pm 3.2 M_\oplus$  ( $M_p < 15.4 M_\oplus$  at 98% confidence) compared to the previously reported  $M_p = 24.5 \pm 4.4 M_\oplus$ . While the true cause of the original mass measurement’s inaccuracy remains uncertain, we present the plausible explanation that the planet’s radial velocity (RV) semi-amplitude was inflated due to constructive interference with a second, untreated sinusoidal signal in the data (possibly rotational modulation from the star). HD 119130 b illustrates the complexities of interpreting the RV orbits of small transiting planets. While RV mass measurements of such planets may be precise, they are not necessarily guaranteed to be accurate. This system serves as a cautionary tale as observers and theorists alike look to the exoplanet mass-radius diagram for insights into the physics of small planet formation.

*Keywords:* Exoplanets (498), radial velocity (1332)

### 1. INTRODUCTION

Luque et al. (2019, hereafter L19) reported the discovery and confirmation of the sub-Neptune-size planet HD 119130 b (aka K2-292 b). L19 detected the planet’s transits in *K2* photometry (Howell et al. 2014) and sub-

sequently conducted RV follow-up with the Calar Alto high-Resolution search for M dwarfs with Exoearths with Near-infrared and optical Échelle Spectrographs (CARMENES; Quirrenbach et al. 2014, 2018). HD 119130 b orbits its G dwarf host every 17 days. Jointly modeling the four *K2* transits and their 18 CARMENES RVs, the authors found  $R_p = 2.63_{-0.10}^{+0.11} R_\oplus$  and  $M_p = 24.5 \pm 4.4 M_\oplus$ , making this planet unusually massive for its size. At the time of its publication, HD 119130 b

Corresponding author: Joseph M. Akana Murphy  
joseph.murphy@ucsc.edu

\* NSF Graduate Research Fellow

† NHFP Sagan Fellow

was one of only two<sup>1</sup> planets with  $M_p \geq 20 M_\oplus$  and  $R_p \leq 3 R_\oplus$  (the other being K2-66 b, a planet in the photoevaporation desert orbiting a subgiant star; [Sinukoff et al. 2017](#)).

Given its curiously high bulk density of  $\rho_p = 7.4_{-1.5}^{+1.6}$  g cm<sup>-3</sup>, L19 dubbed HD 119130 b a rare “ultra-dense” sub-Neptune. The authors posited that the planet must have formed with high density since it is too weakly irradiated ( $S_p = 67 S_\oplus$ ) to have lost a massive primordial envelope via photoevaporation (e.g., [Owen & Wu 2013](#)). Furthermore, the inner disk of the planet’s G dwarf host would not have contained sufficient material to form a  $20 M_\oplus$  planet in situ at 0.1 au ([Schlichting 2014](#)), meaning HD 119130 b must have formed beyond the snow line and migrated inward over time—possibly in lockstep with the snow line itself ([Kennedy & Kenyon 2008](#)). L19 suggested that the migration could have been caused by Kozai-Lidov oscillations ([Dawson & Chiang 2014](#); [Mustill et al. 2017](#)), which may have been triggered by a potential long-period companion associated with their detection of a linear RV trend. In this context, ultra-dense sub-Neptunes may represent a valuable tracer of protoplanetary disk composition beyond the snow line, and their orbital architectures could lend insights into the physics of planet migration.

Since the confirmation of HD 119130 b, other ultra-dense or “superdense” sub-Neptunes have appeared in the literature, including K2-182 b ([Akana Murphy et al. 2021](#)) and HD 21749 b ([Dragomir et al. 2019](#); [Gan et al. 2021](#)). To date, there are only eight planets (not including HD 119130 b) with  $M_p \geq 20 M_\oplus$  and  $R_p \leq 3 R_\oplus$ , whose masses were measured using RVs.<sup>2</sup> There are another three such planets with masses derived from transit timing variations (TTVs; e.g., [Hadden & Lithwick 2014](#)).

As with any collection of seemingly unusual planets—for example, planets lying in the photoevaporation desert (e.g., [Szabó & Kiss 2011](#); [Lundkvist et al. 2016](#); [Armstrong et al. 2020](#)) or the so-called “super-puffs” (e.g., [Lee & Chiang 2016](#); [Jontof-Hutter 2019](#); [Libby-Roberts et al. 2020](#))—it is natural to wonder if these objects truly represent a unique outcome of planet formation, or if the measurements (of the planet masses, in particular) are the product of some conspiracy between observational biases and model misspecification. [Lange](#)

[et al. \(2024\)](#) find that the majority of superdense sub-Neptunes with mass measurements from RV monitoring were confirmed using less than 30 observations. Superdense sub-Neptunes may be particularly vulnerable to publication bias because, for a given measurement uncertainty, a larger mass will lead to a higher-precision detection. This bias may, in turn, serve to influence our understanding of the small planet mass-radius relation ([Burt et al. 2018](#)).

To verify the accuracy of HD 119130 b’s mass measurement, we conducted follow-up Doppler observations as part of the THIRSTEE<sup>3</sup> survey ([Lacedelli et al. 2024](#)). In total, we obtained 57 new RVs of HD 119130. Combined with the CARMENES data from L19, our observations reveal that HD 119130 b is not, in fact, an ultra-dense sub-Neptune. Instead, we find  $M_p = 8.8 \pm 3.2 M_\oplus$  ( $M_p < 15.4 M_\oplus$  at 98% confidence), which is much more typical for a planet of its size. We also find that the data prefer including a low-frequency signal, which can either be modeled as an outer planetary-mass companion with  $P \approx 200$  days and  $K = 4.9 \pm 1.2$  m s<sup>-1</sup>, or as a long-term linear trend. We explore possible explanations for the original mass measurement’s inaccuracy, including untreated stellar activity and imperfect time-sampling.

The paper is organized as follows. In §2, we describe our observations. In §3, we present our RV analysis and revised mass measurement for HD 119130 b. In §4, we explore possible explanations for the inaccuracy of the L19 mass measurement. In §5, we discuss the planet’s possible composition and formation and evolution scenarios in the context of its revised mass estimate. We conclude in §6.

## 2. OBSERVATIONS

Here we summarize the RV observations of HD 119130. The data, including the archival CARMENES RVs from L19, can be found in Table 1.

### 2.1. CARMENES

L19 obtained 18 RVs from CARMENES between UT 2018 Jun 14 and 2018 Jul 18. The CARMENES RVs have a median internal uncertainty of 3.1 m s<sup>-1</sup> and an RMS of 7.1 m s<sup>-1</sup> about the mean value.

### 2.2. HARPS

The High-Accuracy Radial velocity Planetary Searcher (HARPS; [Mayor et al. 2003](#)) is an ultra-precise optical Échelle spectrograph with sub-ms<sup>-1</sup> precision installed at the European Southern Observatory (ESO)

<sup>1</sup> According to the data from the TEPcat catalog ([Southworth 2011](#)) as shown in Figure 6 from L19.

<sup>2</sup> According to the NASA Exoplanet Archive’s Planetary Systems Table, as accessed on 2024 Sept 02 ([NASA Exoplanet Archive 2024](#)), for planets with better than 33% and 15% fractional measurement precision in mass and radius, respectively.

<sup>3</sup> Tracking Hydrates In Refined Sub-neptunes to Tackle their Emergence and Evolution.

3.6 m telescope at La Silla Observatory in Chile. We obtained 31 high-resolution spectra between UT 2023 Apr 02 and 2023 Jul 09 under program 0111.C-0138 (PI: E. Pallé). Besides RV measurements, we extracted the full-width at half maximum (FWHM) and bisector span (BIS) of the cross-correlation function (CCF) from the FITS headers, as computed by the DRS ESO HARPS pipeline. The RVs have a median internal uncertainty of  $2.3 \text{ m s}^{-1}$  and an RMS of  $5.6 \text{ m s}^{-1}$  about the mean value.

### 2.3. HARPS-N

The High-Accuracy Radial velocity Planetary Searcher-North (HARPS-N; Cosentino et al. 2012) spectrograph is mounted at the 3.6 m Telescopio Nazionale Galileo of Roque de los Muchachos observatory in La Palma, Spain. We obtained 16 high-resolution spectra between UT 2023 Apr 13 and 2024 May 13 under the observing programs CAT23A.52 and CAT23B.74 (PI: I. Carleo). RVs and additional spectral indicators were derived from the CCF using an online version of the DRS pipeline (Cosentino et al. 2014), the YABI tool<sup>4</sup>. The RVs have a median internal precision of  $1.9 \text{ m s}^{-1}$  and an RMS of  $4.3 \text{ m s}^{-1}$  about the mean value.

### 2.4. Keck-HIRES

The High Resolution Echelle Spectrometer (HIRES; Vogt et al. 1994) is mounted on the 10 m Keck I telescope at the W. M. Keck Observatory on Maunakea, Hawai‘i. We obtained 10 high-resolution spectra of HD 119130 between UT 2023 Apr 10 and 2023 Jun 25 under observing program 2023A\_U156 (PI: N. Batalha). For these observations, a warm ( $50^\circ \text{ C}$ ) cell of molecular iodine was placed at the entrance slit (Butler et al. 1996). The superposition of the iodine absorption lines on the stellar spectrum provides both a fiducial wavelength solution and a precise, observation-specific characterization of the instrument’s point spread function (PSF). To measure precise RVs using the iodine method, a high-resolution, high-S/N, iodine-free “template” spectrum must also be obtained to create a deconvolved stellar spectral template (DSST) of the host star. We obtained the iodine-free template of HD 119130 on UT 2023 Jun 24. The data collection and reduction followed the methods of the California Planet Search (CPS) as described in Howard et al. (2010). The RVs have a median internal precision of  $1.5 \text{ m s}^{-1}$  and an RMS of  $2.5 \text{ m s}^{-1}$  about the mean value.

<sup>4</sup> Available at <http://ia2-harps.oats.inaf.it:8000>.

**Table 1.** HD 119130 RVs

| Time        | RV                    | RV Unc.               | Inst.    |
|-------------|-----------------------|-----------------------|----------|
| [BJD]       | [ $\text{m s}^{-1}$ ] | [ $\text{m s}^{-1}$ ] |          |
| 2458284.416 | 0.86                  | 2.14                  | CARMENES |
| ...         | ...                   | ...                   | ...      |

NOTE—The complete set of 75 RVs (i.e., the 18 observations from Luque et al. 2019 plus the 57 new observations published in this work) used in our analysis of HD 119130. Only the first row of the table is shown here to inform its contents and format. BJD is reported using the TDB standard (e.g., Eastman et al. 2010). Model-specific instrumental offsets have not been applied to the RV values listed here. The RV errors listed here represent measurement uncertainty and have not been added in quadrature with the corresponding instrument jitter values resulting from our models of the data. This table is available in its entirety online in machine-readable format.

## 3. ANALYSIS

### 3.1. Reproducing the L19 results

First, we attempted to reproduce the results from L19 by restricting ourselves to the 18 CARMENES RVs and replicating their RV analysis. L19 find  $K = 6.1 \pm 1.1 \text{ m s}^{-1}$  and  $e = 0.04_{-0.03}^{+0.06}$  for HD 119130 b as part of a joint model with the *K2* photometry. We only analyzed the CARMENES RVs (i.e., we did not recreate a joint model that included the *K2* photometry) but placed informed Gaussian priors on the orbital period ( $P$ ) and time of inferior conjunction ( $T_{\text{conj}}$ ) of HD 119130 b using the posterior estimates from L19. All other model parameters had wide, uninformed priors. To guard ourselves against potential systematic biases between analysis tools, we fit the data using two separate modeling codes, *RadVel* (Fulton et al. 2018) and *exoplanet* (Foreman-Mackey et al. 2020). Mimicking the L19 RV model, we find that  $K_b$  is consistent to within  $1\sigma$  of the L19 value for both codes.

### 3.2. Model comparison

After reproducing the results from L19, we turned our attention to analyzing the entire RV time series from all four instruments. We compared different models of the data using the small sample corrected Akaike Information Criterion (AICc; Akaike 1974; Burnham & Ander-

son 2002). The AICc is defined as

$$\text{AICc} = \text{AIC} + \frac{2N_{\text{par}}(N_{\text{par}} + 1)}{N_{\text{obs}} - N_{\text{par}} - 1}, \quad (1)$$

and the Akaike Information Criterion (AIC; Akaike 1974) is given as

$$\text{AIC} = 2N_{\text{par}} - 2 \ln \hat{\mathcal{L}}. \quad (2)$$

$N_{\text{par}}$  is the number of free model parameters,  $N_{\text{obs}}$  is the number of observations, and  $\hat{\mathcal{L}}$  is the model’s likelihood function maximized with respect to the model parameters. Throughout, we assume a log-likelihood of the form

$$\ln \mathcal{L} = -\frac{1}{2} \sum_{i=1}^{N_{\text{obs}}} \left[ \ln(2\pi\sigma_{i, \text{tel}}^2) + \frac{(x_i - \mu_{i, \text{tel}})^2}{\sigma_{i, \text{tel}}^2} \right], \quad (3)$$

where  $x_i$  is the RV of the  $i$ -th observation taken at time  $t_i$ . We define

$$\sigma_{i, \text{tel}}^2 = \sigma_i^2 + \sigma_{\text{jit, tel}}^2, \quad (4)$$

where  $\sigma_i$  is the measurement uncertainty on the  $i$ -th observation and  $\sigma_{\text{jit, tel}}$  is the corresponding RV jitter parameter for the instrument that produced the observation. The model’s predicted RV at time  $t_i$  is given as

$$\mu_{i, \text{tel}} = \text{Keplerian}(t_i, P, T_c, e, \omega_p, K) + \gamma_{\text{tel}} \quad (5)$$

where  $\text{Keplerian}(\dots)$  is the sum of the RV contributions from all of the Keplerian orbits considered by the model and  $\gamma_{\text{tel}}$  is the corresponding instrument-specific RV offset.

While there are no hard and fast rules that dictate model selection with the AIC (or AICc), Burnham & Anderson (2004) provide the following guidelines for comparing the AIC of a reference model,  $\text{AIC}_0$ , and of some other model,  $\text{AIC}_i$ :

- If  $\text{AIC}_i - \text{AIC}_0 \equiv \Delta\text{AIC}_i < 2$ , the two models are nearly indistinguishable.
- If  $2 < \Delta\text{AIC}_i < 10$ , the  $i$ th model is disfavored.
- If  $\Delta\text{AIC}_i > 10$ , the  $i$ th model is ruled out.

The AICc is essentially the same as the AIC, but with an additional penalty term for model complexity, since the AIC has a tendency to favor models that overfit when  $N_{\text{obs}}$  is small. Burnham & Anderson (2002) recommend using the AICc in place of the AIC when  $N_{\text{obs}} \lesssim 40 \times N_{\text{par}}$ , which is typically the case for models of RVs, where  $N_{\text{par}}$  is usually on the order of 10 and  $N_{\text{obs}} \lesssim 100$ .

### 3.3. Selecting a baseline model

To model the orbit of HD 119130 b, we placed an informed Gaussian prior on  $P$  using the posterior estimate from L19. Assuming a linear ephemeris and propagating the L19 value for  $T_{\text{conj}}$  to near the median of the HARPS, HARPS-N, and HIRES RV observations,  $T_{\text{conj}} = 2460235.4 \pm 0.1$  BJD. Given the long gap in time between the *K2* transits and our RV follow-up, we elected to place a uniform prior on  $T_{\text{conj}}$  with a width of  $\pm 8$  days, centered at the propagated L19 value. We found that models performed better when using this wider prior on  $T_{\text{conj}}$ , as opposed to a Gaussian corresponding to the formally propagated uncertainty. The AICc did not prefer an eccentric orbit for HD 119130 b, and an eccentric orbit did not affect the planet’s measured mass, so we enforced a circular orbit. A maximum a posteriori (MAP) fit of the data results in  $K_b = 2.20$  m s<sup>-1</sup>.

After subtracting the orbit of planet b from the data, we computed a Generalized Lomb-Scargle (GLS; Zechmeister & Kürster 2009) periodogram of the residuals. In the GLS periodogram, we find an envelope of peaks, centered at  $P \approx 200$  days, rising above the 0.1% false-alarm probability (FAP; Baluev 2008) threshold. Fitting a second circular Keplerian orbit to the data, we find a candidate signal with  $P = 200.3$  days and  $K = 4.9$  m s<sup>-1</sup>. A GLS periodogram of the data after removing this second signal does not produce any peaks that meet the 0.1% FAP level. GLS periodograms of the data and residuals are shown in Figure 1. The AICc did not prefer an eccentric orbit for the  $P = 200$  days signal, and including an eccentric orbit for the outer signal did not affect the mass of planet b.

What is the nature of this second signal? In both the CARMENES and the HARPS RVs, the data contain a linear trend of similar slope that is inconsistent with the orbit of planet b. L19 account for the trend in the CARMENES data by adding a linear drift term ( $\dot{\gamma}$ ) to their RV model, and suggest that it may indicate the presence of an outer companion. With our larger data set spanning a much longer baseline, this slope is subsumed by the Keplerian orbit with  $P \approx 200$  days. For completeness, we tested a one-planet model that included a linear trend. This configuration did not affect the measured RV semi-amplitude of planet b, but it was ruled out compared to a two-Keplerian fit, with  $\Delta\text{AICc} > 30$ .

Comparing a one- and two-Keplerian model using the AICc, we find that a two-Keplerian model is preferred at the  $\Delta\text{AICc} = 24$  level. We do not claim that this second signal is planetary—additional data are required to reveal its true nature—but it is clear that a single-planet

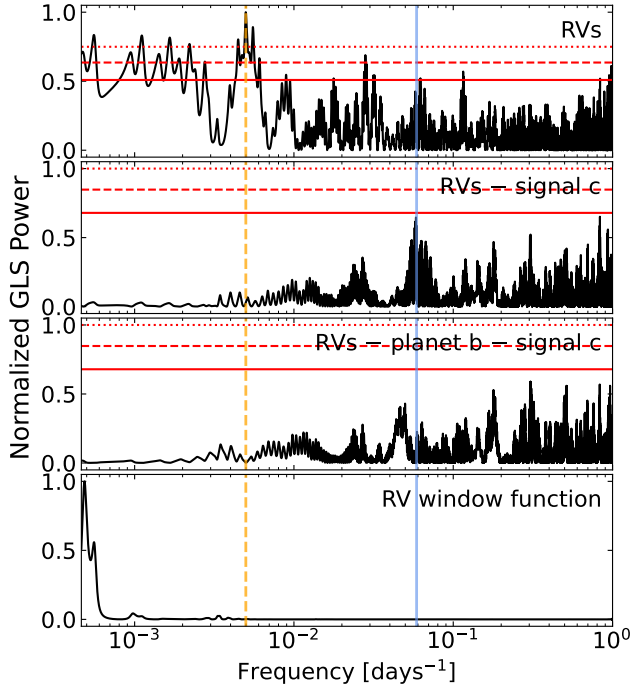


**Figure 1.** GLS periodograms of the HD 119130 RVs (minus instrumental offsets), RV residuals, and RV window function. The solid (dashed) blue (orange) vertical line corresponds to the period of planet b (signal c). The dotted, dashed, and solid red horizontal lines correspond to the 0.1, 1, and 10% FAP thresholds, respectively, for each periodogram, as computed following [Baluev \(2008\)](#).

solution does not adequately describe the data. Moving forward, we consider this circular, two-Keplerian configuration as our “baseline” model. The model parameters and priors are described in [Table 2](#).

### 3.4. A systematic search for additional signals

After identifying a baseline RV model for HD 119130, we then used *RVSearch* ([Rosenthal et al. 2021](#)) to systematically search the RV residuals for additional periodicity. *RVSearch* compared our baseline, circular, two-Keplerian model to a series of three-Keplerian models, defined by a grid of orbital periods for the third Keplerian. The period grid bounds were 2 days and  $5 \times \tau$ , with  $\tau$  being the observational baseline, in days, of the RV data (in our case,  $\tau = 2160$  days). The grid was sampled such that in frequency-space, adjacent grid points were spaced by  $(2\pi\tau)^{-1}$ , corresponding to the minimum peak width found in a Lomb-Scargle periodogram ([Lomb 1976](#); [Scargle 1982](#)) of unevenly sampled time series data ([Horne & Baliunas 1986](#)).

*RVSearch* computed the difference in the Bayesian information criterion (BIC; [Schwarz 1978](#)) between the two- and three-Keplerian models. The BIC is defined

**Table 2.** The HD 119130 RV model

| Parameter [units]  | Prior                                       |
|--|---|
| <i>Planet b</i>  |   |
| $P$ [days]   | $\mathcal{N}(16.9841, 0.0008)$              |
| $T_{\text{conj}}$ [BJD]                                  | $\mathcal{U}[T_{0,b} - 8, T_{0,b} + 8]$     |
| $e$  | $\equiv 0$                                  |
| $\omega_p$ [rad]   | $\dots$                                     |
| $K$ [ $\text{m s}^{-1}$ ]                                | $\mathcal{U}[0, 100]$                       |
| <i>Signal c</i>  |   |
| $P$ [days]   | $\mathcal{U}[P_{0,c} - 20, P_{0,c} + 20]$   |
| $T_{\text{conj}}$ [BJD]                                  | $\mathcal{U}[T_{0,c} - 100, T_{0,c} + 100]$ |
| $e$  | $\equiv 0$                                  |
| $\omega_p$ [rad]   | $\dots$                                     |
| $K$ [ $\text{m s}^{-1}$ ]                                | $\mathcal{U}[0, 100]$                       |
| <i>Instrument parameters</i>                             |   |
| $\gamma_{\text{tel}}$ [ $\text{m s}^{-1}$ ]              | $\mathcal{U}[-250, 250]$                    |
| $\ln \sigma_{\text{jit, tel}}$ [ $\ln \text{m s}^{-1}$ ] | $\mathcal{U}[-3, 6]$                        |

NOTE— $\mathcal{N}(X, Y)$  refers to a Gaussian distribution with mean  $X$  and standard deviation  $Y$ .  $\mathcal{U}[X, Y]$  refers to a uniform distribution on the interval  $X$  and  $Y$ . The uniform prior on the time of inferior conjunction for planet b is centered on  $T_{0,b} = 2460235.4$  BJD, which comes from propagating the L19 transit time to near the middle of the observing baseline for the RVs collected in 2023 and 2024, assuming a linear ephemeris. The uniform prior on the orbital period of candidate signal c is centered on  $P_{0,c} = 200$  days, which represents the largest peak in a periodogram of the one-planet residuals. The center of the prior on the time of inferior conjunction of candidate signal c,  $T_{0,c}$ , is arbitrarily chosen to be the median of the RV time series. There are offset and RV jitter parameters ( $\gamma_{\text{tel}}$  and  $\sigma_{\text{jit, tel}}$ , respectively) for each instrument. We fit the natural logarithm of  $\sigma_{\text{jit, tel}}$  to avoid pathological posterior geometries known to cause issues for Hamiltonian Monte Carlo-based samplers ([Neal 2003](#); [Betancourt & Girolami 2015](#)).

as

$$\text{BIC} = N_{\text{par}} \ln N_{\text{obs}} - 2 \ln \hat{\mathcal{L}}, \quad (6)$$

where notation is the same as before. Using the detection methodology described by Howard & Fulton (2016), RVSearch then estimated the  $\Delta\text{BIC}$  value corresponding to an FAP threshold of 0.1%. In our case, we find that  $\Delta\text{BIC} = 52.1$  corresponds to  $\text{FAP} = 0.1\%$ . Since none of the three-Keplerian models resulted in a  $\Delta\text{BIC}$  value that exceeded the 0.1% FAP threshold, we adopted the two-Keplerian solution moving forward.

To get a sense of the range of signals that could be present in the data but fall below our detection threshold, we used RVSearch to conduct a series of injection-recovery tests (Figure 2). To run an injection-recovery test, we randomly sampled (uniformly in log-log space) an orbital period and an RV semi-amplitude value from a grid spanning  $P \in [2, 5 \times \tau]$  days and  $K \in [0.5, 50]$   $\text{m s}^{-1}$ . We then added the corresponding signal to the RVs assuming a circular Keplerian orbit and computed the  $\Delta\text{BIC}$  between the two- and three-Keplerian models of the augmented data. If the  $\Delta\text{BIC}$  between the models exceeded the  $\text{FAP} = 0.1\%$  threshold, we considered the additional signal to be successfully recovered. We repeated this procedure for 3,000 pairs of  $P$  and  $K$ .

For  $P < 70$  days (i.e., the baseline of the *K2* observations), we find that the data are not sensitive ( $\lesssim 50\%$  recovery rate) to Keplerians with  $K \lesssim 5 \text{ m s}^{-1}$ . L19 conducted a box least squares (BLS; Kovács et al. 2002) search of the *K2* photometry, but found no transiting planet candidates other than HD 119130 b, meaning that any additional planets in the system with  $P < 70$  days are likely non-transiting. For a planet with  $P = 35$  days on a circular orbit,  $b > 1$  implies  $i_p < 88.6^\circ$ , which is consistent with the inclination of HD 119130 b ( $i_p = 88.4 \pm 0.3^\circ$ ). This means that requiring such a planet to be non-transiting does not necessarily imply that it must also have a large mutual inclination with HD 119130 b. For  $P = 35$  days and  $e = 0$ ,  $K < 5 \text{ m s}^{-1}$  corresponds to  $M_p \sin i_p \lesssim 26 M_\oplus$  (at  $P = 70$  days and all else equal, the limit is  $M_p \sin i_p \lesssim 32 M_\oplus$ ). Assuming near-coplanarity between any outer non-transiting companions and planet b, these upper limits are consistent with the masses of sub-Neptune- and Neptune-sized planets.

### 3.5. Stellar activity

Stellar activity is known to confound planet detection with RVs, especially when planetary orbits coincide with the stellar rotation period or its harmonics (e.g., Vanderburg et al. 2016). Untreated stellar activity signals in RV time series can also lead to mass measurement inaccuracy (Rajpaul et al. 2017). As such, we investigated

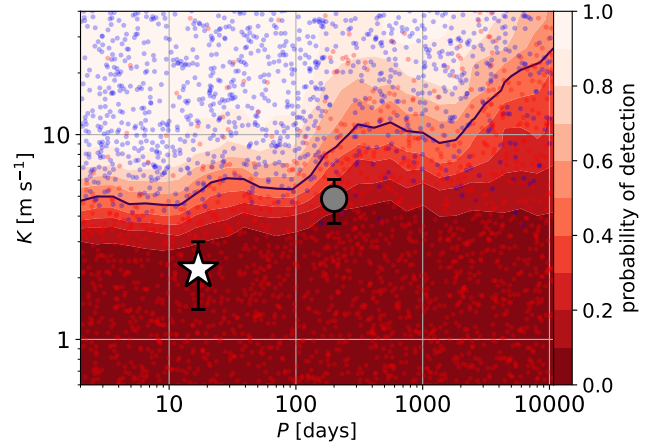


**Figure 2.** Sensitivity map for our injection-recovery tests on the HD 119130 RV data using RVSearch. Points represent individual  $P$  and  $K$  combinations that were injected into the RV residuals. Blue points correspond to signals that were successfully recovered after removing the orbit of HD 119130 b and the candidate signal at  $P \approx 200$  days, while red points correspond to signals that were not recovered. Signals were considered “recovered” if their corresponding peak in a periodogram of the residuals rose above the 0.1% FAP threshold, as determined following the methods of Howard & Fulton (2016). The results of the individual injections and recovery searches were used to compute the contours, which correspond to detection probability (see colorbar). The solid black line corresponds to a detection efficiency of 50%. The white star represents HD 119130 b and the gray circle represents the outer candidate, signal c.

HD 119130’s activity signatures before adopting a final RV model.

HD 119130 is a chromospherically-inactive, slowly-rotating, G3V dwarf (Houk & Swift 1999). Following the methods of Isaacson et al. (2024), we measured  $\log_{10} R'_{\text{HK}} = -5.08 \pm 0.05$  using our Keck-HIRES iodine-free template spectrum. From the Keck-HIRES template we also found  $v \sin i_* < 2 \text{ km s}^{-1}$  using the SpecMatch-Synth tool (Petigura et al. 2017). This measurement is consistent at the  $3\sigma$ -level with the value from L19 of  $v \sin i_* = 4.6 \pm 1.0 \text{ km s}^{-1}$ . Assuming the stellar obliquity is zero (i.e.,  $i_* = i_p = 88.4 \pm 0.3^\circ$ ) our upper limit on  $v \sin i_*$  corresponds to  $P_{\text{rot}} > 27.6$  days, while the value from L19 translates to  $P_{\text{rot}} = 12.0 \pm 2.6$  days.

To check for photometric variability indicative of star spots, we extracted the *K2* Campaign 17 light curve using the everest pipeline (Luger et al. 2018). After removing the in-transit flux, we followed the methods described in Akana Murphy et al. (2021) to clean the data with a Savitsky-Golay filter (Savitzky & Golay 1964). We did not find any evidence of an obvious stellar rotation period in the cleaned, out-of-transit flux time series,

or in a GLS periodogram of the *K2* data. We note that NASA’s Transiting Exoplanet Survey Satellite (TESS; Ricker et al. 2014) has not observed HD 119130 as of Cycle 7.

To check for signs of stellar activity in the spectroscopic data, we examined the HARPS BIS, CCF FWHM, and CCF contrast measurements. The HARPS data was chosen as it represents our largest collection of observations from a single instrument. GLS periodograms of the activity indicator time series are shown in Figure 3. There are no peaks of significant power in the immediate neighborhood of the transiting planet’s orbital period for any of activity indicators.

Despite the lack of an obvious stellar rotation signal in the photometric or spectroscopic data, we added a Gaussian process (GP; e.g., Rasmussen & Williams 2006) to our two-Keplerian RV model in an effort to remove any correlated noise related to activity. We implemented the model with *RadVel*. For the GP we used the quasi-periodic (QP) kernel (e.g., Grunblatt et al. 2015; Kosiarek et al. 2021), which, for each instrument,  $i$ , quantifies covariance between data observed at times  $t$  and  $t'$  as

$$k_i(t, t') = \eta_{1,i}^2 \exp \left[ -\frac{(t - t')^2}{\eta_2^2} - \frac{\sin^2\left(\frac{\pi(t-t')}{\eta_3}\right)}{2\eta_4^2} \right]. \quad (7)$$

$\eta_{1-4}$  are the hyperparameters:  $\eta_{1,i}$  represents the amplitude of the covariance for instrument  $i$ ,  $\eta_2$  is interpreted as the evolutionary timescale of active stellar regions,  $\eta_3$  is interpreted as the stellar rotation period, and  $\eta_4$  is the length scale of the covariance’s periodicity. The hyperparameters are shared between instruments save for the amplitudes,  $\eta_{1,i}$ . Before adding the GP to a model of the RVs, we first trained the GP by fitting it to the HARPS BIS values, which seemed to produce the most well-formed posteriors on the hyperparameters compared to the other activity indicators. The posteriors of  $\eta_2$ ,  $\eta_3$ , and  $\eta_4$  resulting from the training were then used as numerical priors when conducting the MAP fit of the RVs.

The two-Keplerian plus GP model finds  $K_b = 2.3 \text{ m s}^{-1}$ , which matches the result of the Keplerian-only fit ( $K_b = 2.2 \text{ m s}^{-1}$ ). For the periodic time scale of the GP, the MAP fitting finds  $\eta_3 = 23.8 \text{ days}$ , which is about twice the  $P_{\text{rot}}$  estimate implied by the  $v \sin i_*$  value from L19. While this may seem to suggest that the GP has found the stellar rotation signal (or one of its aliases), the semi-amplitude of planet b remains agnostic. The GP model, with its seven additional parameters (21 free parameters in total), is ruled out by the AICc ( $\Delta\text{AICc} = 18$ ) when compared to the Keplerian-only model. GPs are also prone to overfitting (Blunt et al.

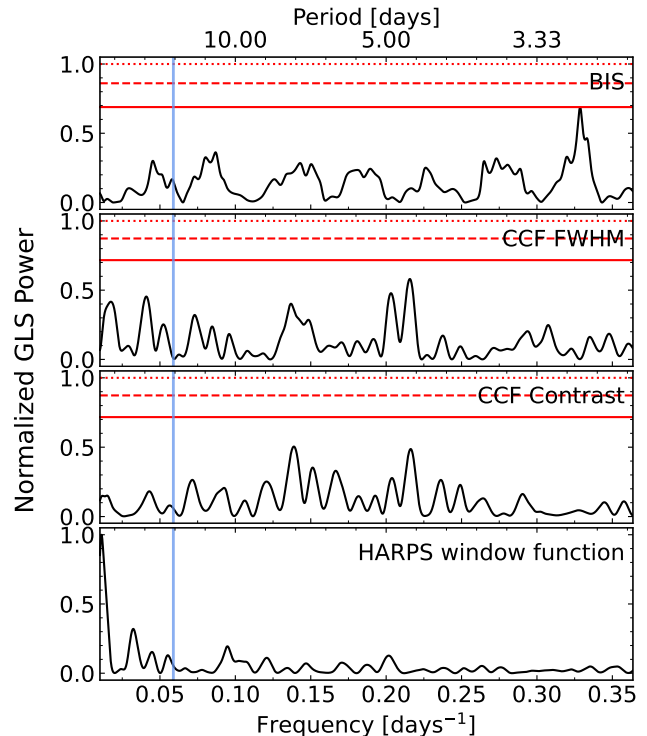


**Figure 3.** GLS periodograms of the HARPS activity indices and window function. The HARPS data comprise 31 spectra obtained over a baseline of 98 days. The solid blue vertical line corresponds to the orbital period of planet b. The dotted, dashed, and solid red horizontal lines correspond to the 0.1, 1, and 10% FAP thresholds, respectively, for each periodogram, as computed following Baluev (2008).

2023), so while a stellar activity signal may be present in the existing data, more observations are required before a GP-enabled analysis is warranted. In any case, the inclusion of a GP does not affect the semi-amplitude of planet b.

### 3.6. Adopted RV model and posterior estimates

To produce our final measurements of the orbit and mass of HD 119130 b, we fit the full RV data set in *exoplanet* using our baseline, circular, two-Keplerian model (Table 2). Observations from the same telescope falling within 8 hours of each other were binned together, resulting in 29 binned HARPS RVs (compared to 31 unbinned RVs) and 15 binned HARPS-N RVs (compared to 16) for the model. The adopted RV model is shown in Figure 4 and system parameters are summarized in Table 3.

To estimate the posterior distributions of the model parameters we used a No-U-Turn Sampler (NUTS; Hoffman & Gelman 2014), an adaptive form of Hamiltonian Monte Carlo (HMC; Duane et al. 1987; Neal 2012), implemented with *pymc3* (Salvatier et al. 2016). The

NUTS ran 8 parallel chains with each chain taking 8,000 tuning steps before drawing 2,000 samples. Samples drawn during the tuning period were discarded, similar to how various Markov Chain Monte Carlo (MCMC) methods discard burn-in samples. The chains were concatenated to produce a total of 16,000 samples from the posterior of each model parameter. We computed the rank-normalized Gelman-Rubin statistic ( $\hat{R}$ ; Gelman & Rubin 1992; Vehtari et al. 2021) for the chains and find  $\hat{R} < 1.001$  for all model parameters, suggesting convergence. We also computed the rank-normalized effective sample sizes of the bulk and tails of each posterior distribution (Vehtari et al. 2021) and find that they are all sufficiently large ( $N_{\text{eff}} > 1000$ ) compared to the recommended threshold ( $N_{\text{eff}} = 400$ ).

#### 4. UNDERSTANDING THE MASS MEASUREMENT INACCURACY

##### 4.1. Sanity checks

Why is the L19 mass measurement inaccurate? Before exploring possible explanations, we conduct two brief sanity checks to further convince the reader that the discrepancy between our measurement and the L19 value cannot be explained by systematic differences in our analysis. First, we compared the HARPS and HARPS-N data—which have a similar sampling cadence compared to the CARMENES RVs—to the orbital solution from L19. It is clear by eye that the new data do not agree with the orbit (see Figure 5). The RMS of the HARPS and HARPS-N data about the L19 orbit is  $7.3 \text{ m s}^{-1}$ , compared to  $4.0 \text{ m s}^{-1}$  for all of the data about our adopted solution.

Second, if HD 119130 b did indeed have  $K_b = 6 \text{ m s}^{-1}$ , the signal would have been easily detected in our data given our number of measurements, sampling cadence, observing baseline, and typical measurement uncertainty. Using the L19 orbital solution, we generated synthetic RV measurements at our observation time stamps with a measurement uncertainty of  $2.5 \text{ m s}^{-1}$  (the average measurement uncertainty of our data) and  $3 \text{ m s}^{-1}$  of additional white noise added in quadrature (the average of the best-fitting RV jitter values across the four instruments). The GLS periodogram of the synthetic time series is shown in the top panel of Figure 6. In this case, the planet is easily detected with an FAP of much less than 0.1%. Of course, this simulation assumes that the transiting planet is the only periodic signal present in the data.

##### 4.2. Observing cadence and number of measurements

**Table 3.** HD 119130 system properties

| Parameter [units]                         | Value                  | Provenance      |
|---|------------------------|-----------------|
| <i>System information</i>                 |                        |                 |
| EPIC ID                                   | 212628254              | EPIC            |
| TIC ID                                    | 124573851              | Guerrero        |
| R.A. [J2000]                              | 13:41:30.2             | <i>Gaia</i> DR3 |
| decl. [J2000]                             | −09:56:45.9            | <i>Gaia</i> DR3 |
| Parallax [mas]                            | $8.81 \pm 0.02$        | <i>Gaia</i> DR3 |
| $V$ [mag]                                 | $9.92 \pm 0.01$        | Munari          |
| $J$ [mag]                                 | $8.73 \pm 0.02$        | 2MASS           |
| <i>Stellar parameters</i>                 |                        |                 |
| $T_{\text{eff}}$ [K]                      | $5725 \pm 65$          | L19             |
| $\log_{10} g$                             | $4.30 \pm 0.15$        | L19             |
| $v \sin i_*$ [km s $^{-1}$ ]              | $< 2$                  | This work       |
| $v \sin i_*$ [km s $^{-1}$ ]              | $4.6 \pm 1.0$          | L19             |
| $M_*$ [ $M_{\odot}$ ]                     | $1.00 \pm 0.03$        | L19             |
| $R_*$ [ $R_{\odot}$ ]                     | $1.09 \pm 0.03$        | L19             |
| $\log_{10} R'_{\text{HK}}$                | $-5.08 \pm 0.05$       | This work       |
| <i>Planet b measured quantities</i>       |                        |                 |
| $P$ [days]                                | $16.9841 \pm 0.0008$   | L19             |
| $T_c$ [BJD]                               | $2460232.8 \pm 0.9$    | This work       |
| $K$ [m s $^{-1}$ ]                        | $2.2 \pm 0.8$          | This work       |
| $e$                                       | $\equiv 0$             | This work       |
| $\omega_p$                                | $\dots$                | This work       |
| <i>Planet b derived quantities</i>        |                        |                 |
| $a$ [au]                                  | $0.13 \pm 0.01$        | L19             |
| $T_{\text{eq}}$ [K]                       | $795^{+33}_{-28}$      | L19             |
| $T_{\text{dur}}$ [hr]                     | $3.66^{+0.07}_{-0.08}$ | L19             |
| $i_p$ [deg]                               | $88.4^{+0.2}_{-0.3}$   | L19             |
| $R_p$ [ $R_{\oplus}$ ]                    | $2.63^{+0.11}_{-0.10}$ | L19             |
| $M_p$ [ $M_{\oplus}$ ]                    | $8.8 \pm 3.2$          | This work       |
| $\rho_p$ [g cm $^{-3}$ ]                  | $2.7 \pm 1.0$          | This work       |
| <i>Instrument parameters</i>              |                        |                 |
| $\gamma_{\text{CARMENES}}$ [m s $^{-1}$ ] | $-0.3 \pm 3.2$         | This work       |
| $\sigma_{\text{CARMENES}}$ [m s $^{-1}$ ] | $4.8 \pm 1.4$          | This work       |
| $\gamma_{\text{HARPS}}$ [m s $^{-1}$ ]    | $-0.7 \pm 1.0$         | This work       |
| $\sigma_{\text{HARPS}}$ [m s $^{-1}$ ]    | $2.7 \pm 0.8$          | This work       |
| $\gamma_{\text{HARPS-N}}$ [m s $^{-1}$ ]  | $1.4 \pm 1.0$          | This work       |
| $\sigma_{\text{HARPS-N}}$ [m s $^{-1}$ ]  | $2.8 \pm 1.1$          | This work       |
| $\gamma_{\text{HIRES}}$ [m s $^{-1}$ ]    | $-1.7 \pm 1.2$         | This work       |
| $\sigma_{\text{HIRES}}$ [m s $^{-1}$ ]    | $1.7 \pm 1.0$          | This work       |

NOTE— $T_{\text{eq}}$  calculated assuming zero Bond albedo and perfect day-night heat redistribution. References for provenance values: EPIC (Huber et al. 2016), Guerrero (Guerrero et al. 2021), *Gaia* DR3 (Gaia Collaboration et al. 2016, 2023), Munari (Munari et al. 2014), and 2MASS (Skrutskie et al. 2006).

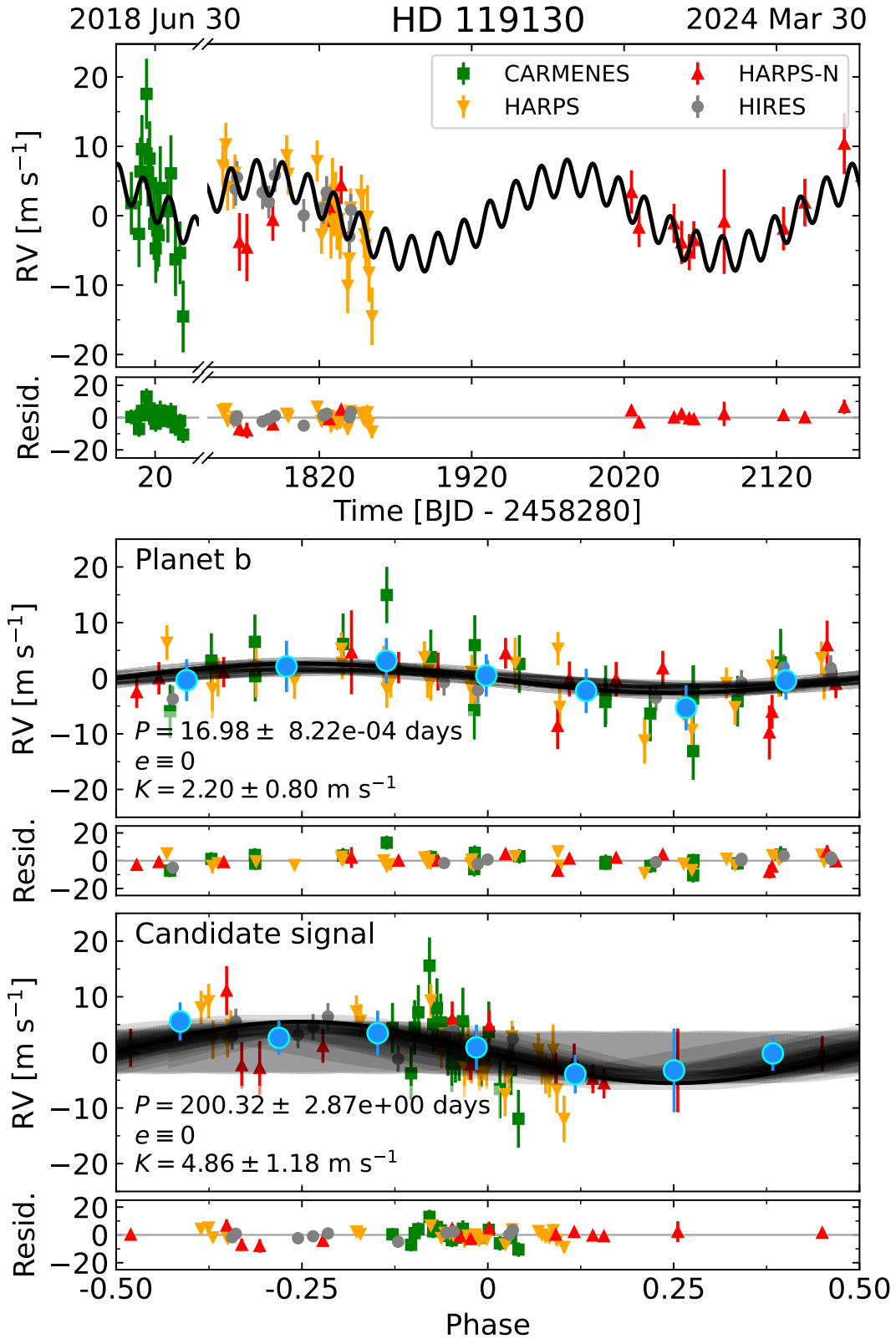


**Figure 4.** The HD 119130 RVs. *Top:* The RV time series (data points with error bars), MAP model (solid black line), and residuals about the MAP solution (lower panel). Note the broken x-axis. *Middle:* The RVs folded to the orbital period of HD 119130 b. RVs binned in units of 0.125 orbital phase are shown as the blue data points. Black lines represent 25 random realizations of the model posterior. Error bars shown represent point wise measurement errors added in quadrature with the associated instrument-specific jitter value that was fit to the data. *Bottom:* The same as above, but for signal c.

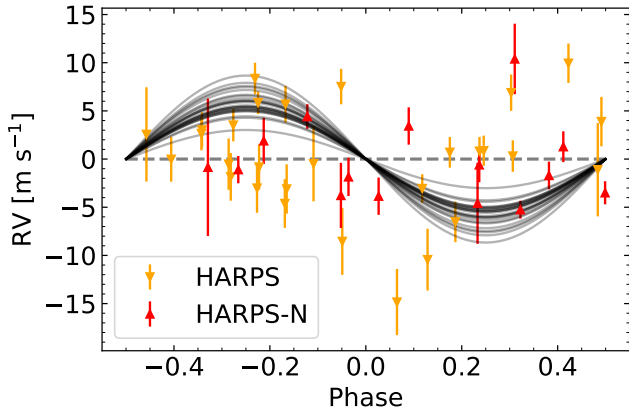


**Figure 5.** The HARPS and HARPS-N data (with instrumental offsets applied) compared to 25 random realizations of HD 119130 b’s orbit, generated using the  $P$ ,  $T_{\text{conj}}$ , and  $K$  values from L19. The new data are inconsistent with the L19 solution.

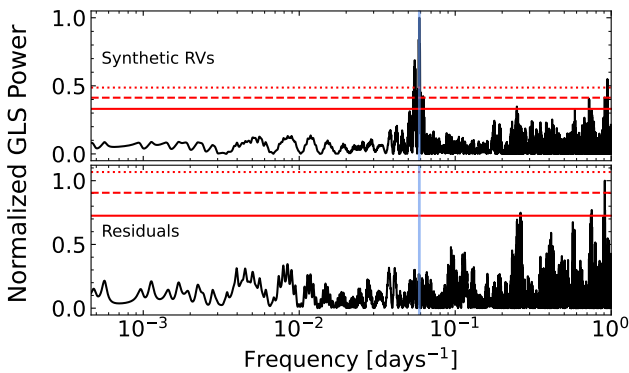


**Figure 6.** *Top:* GLS periodogram of a synthetic RV time series generated by assuming the L19 orbital solution for HD 119130 b and producing an RV at each observation time stamp in our real data set. We assume typical measurement errors and white noise. The vertical blue line marks the orbital period of HD 119130 b. As before, the horizontal lines correspond to the 10%, 1%, and 0.1% FAP thresholds. If the planet did indeed have  $K_b = 6 \text{ m s}^{-1}$ , it would have been easily detected in our data, assuming it is the only periodic signal present. *Bottom:* The residuals of the synthetic RVs after removing the L19 orbit for planet b.

Is the L19 mass measurement’s inaccuracy due to an unfortunate conspiracy between imperfect sampling cadence, observing baseline, and the number of CARMENES observations? Following the methods of Akana Murphy et al. (2024), we resampled the data using different combinations of minimum observing cadence (MOC) and the number of observations in order to visualize how the MAP value of  $K_b$  would change due to these properties alone.

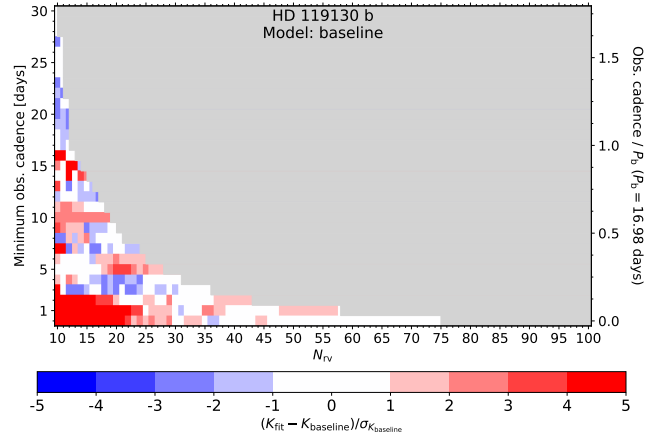


**Figure 7.** The results of the resampling experiment for HD 119130 b following the methods of Akana Murphy et al. (2024). Each cell represents a resampled realization of the full data set according to specified MOC (left y-axis; i.e., a lower limit enforced on the time between consecutive measurements) and  $N_{\text{RV}}$  (x-axis) values. The right y-axis is the same as the left, but it is now shown in units of the orbital period of the planet. The color of each cell represents the difference between the planet’s measured semi-amplitude using that cell’s resampled data set,  $K_{\text{fit}}$ , and the measured semi-amplitude of the planet from the baseline model ( $K_{\text{baseline}}$ ), in units of the uncertainty on  $K_{\text{baseline}}$ . Gray regions represent combinations of minimum observing cadence and  $N_{\text{RV}}$  that are not supported by the data. The right-most, non-gray cell along the bottom row represents the original time series, and is therefore in agreement with  $K_{\text{baseline}}$  by construction.

The results of the resampling experiment are shown in Figure 7. For resampled datasets similar in size to the L19 time series ( $N_{\text{RV}} \approx 20$ ),  $K_b$  can vary widely depending on the chosen MOC. Perhaps this means that the L19 overestimate is a stochastic outcome of the interplay between the sampling cadence of their observations, the orbit of HD 119130 b, and the phase of any additional signals (e.g., stellar activity) present when the CARMENES data were collected.

#### 4.3. Rotational modulation

As discussed in §3.5,  $P \approx 12$  days could plausibly represent the stellar rotation period or its first harmonic (depending on which value of  $v \sin i_*$  is adopted). Is it possible that a coherent stellar rotation signal, interfering constructively with the planetary signal over the course of the L19 observations, was responsible for inflating  $K_b$  from  $2.2 \text{ m s}^{-1}$  to  $6.1 \text{ m s}^{-1}$ ? To test this explanation, we conducted simulations following the methods of Rajpaul et al. (2017).

Using Equation 1 in Rajpaul et al. (2017), we generated synthetic RVs using the observing cadence, number of observations, and noise level of the CARMENES

data. We assumed two sinusoidal signals were present. The first signal corresponded to the RV orbit of planet b:

$$y_{1,i} = K_1 \sin\left(\frac{2\pi t_i}{P_1}\right) + \mathcal{N}(0, \sigma_{\text{CARMENES}}), \quad (8)$$

where  $K_1 = 2.2 \text{ m s}^{-1}$ ,  $P_1 = 16.98 \text{ days}$ ,  $\sigma_{\text{CARMENES}} = 3 \text{ m s}^{-1}$ , and  $t_i$  is the time stamp of the  $i$ -th observation (with the first time stamp arbitrarily set to zero). We then generated 10,000 realizations of a second sinusoid, meant to represent a coherent rotation signal:

$$y_{2,i} = K_2 \sin\left(\frac{2\pi t_i}{P_2} + \phi_2\right) + \mathcal{N}(0, \sigma_{\text{CARMENES}}), \quad (9)$$

where  $K_2 = [1.0, 1.04, \dots, 4.96] \text{ m s}^{-1}$  (an array of 100 elements evenly-spaced between 1–5  $\text{m s}^{-1}$ ) and  $\phi_2 = 2\pi \times [0, 0.01, \dots, 0.99]$  (an array of 100 elements evenly-spaced between 0– $2\pi$  radians).

For each of the 10,000 realizations of the synthetic data,  $y = y_1 + y_2$ , we fit the sinusoid  $y = K \sin\left(\frac{2\pi t}{P}\right)$ , where  $P = 16.98 \text{ days}$ . We recorded the best-fitting  $K$  value for each combination of  $K_2$  and  $\phi_2$ . The results are shown in Figure 8. We see that there are indeed instances where the best-fitting  $K_1$  value is  $\geq 6 \text{ m s}^{-1}$ , though they only account for  $\sim 1\%$  of all trials.  $K_1 \geq 3.9 \text{ m s}^{-1}$  (i.e.,  $K_1 \geq$  the L19 value minus  $2\sigma$ ) accounts for 15% of all trials.

From these statistics alone, the rotational modulation explanation may seem a bit unlikely. But, of course, this experiment was only conducted for one choice of  $P_2$ . In any case, our simple experiment demonstrates that it is at least feasible for a coherent stellar rotation signal on the order of a few  $\text{m s}^{-1}$  to have artificially inflated the RV semi-amplitude of HD 119130 b.

## 5. PLANETARY COMPOSITION, FORMATION, AND EVOLUTION

The mass-radius diagram shown in Figure 9 includes a visual comparison of the drastic change in the mass estimate of HD 119130 b between L19 and this work. How does this new mass measurement change the interpretation of the planet’s bulk composition and formation and evolution history?

Given our relatively imprecise ( $2.75\sigma$ ) constraint on the mass of HD 119130 b, we forgo a detailed analysis of the planet’s interior structure. We note, however, that the new measurement is inconsistent with a pure silicate composition, as previously suggested by L19. The planet’s revised bulk density ( $2.7 \pm 1.0 \text{ g cm}^{-3}$ ) is consistent with a planet comprising an Earth-like core beneath a substantial (1–2% by mass), H/He-dominated volatile envelope or a water-rich core beneath a high-metallicity atmosphere.

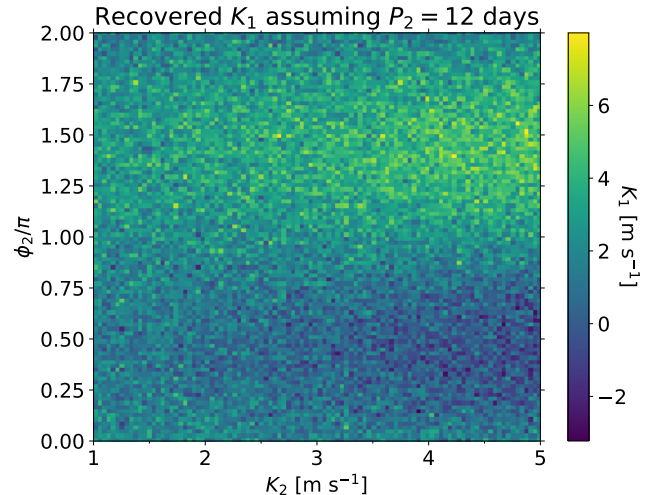


**Figure 8.** A map of best-fitting  $K_1$  values fit using a one-planet model, but where the (synthetic) data contain a second signal at  $P_2 = 12 \text{ days}$ . The second signal is specified by the different combinations of  $K_2$  and  $\phi_2$ . We see that in certain cases,  $K_1$  is inflated to values similar to the result from L19.

Using Equation 15 from [Lecavelier Des Etangs \(2007\)](#), HD 119130 b could lose up to  $0.04 M_{\oplus}$  over 10 Gyr due to extreme ultraviolet radiation from its G dwarf host at its current orbit. According to the grid from [Lopez & Fortney \(2014\)](#), this would translate to a reduction in the planet’s radius by  $\sim 0.2 R_{\oplus}$ . However, even at its lower mass, HD 119130 b would still require a disk mass enhancement factor of  $\sim 30$  above the minimum-mass solar nebula to form at  $a = 0.13 \text{ au}$  (see Equation 7 from [Schlichting 2014](#)), making in situ formation implausible and meaning that the mass loss predicted above is likely an overestimate. As L19 concluded, HD 119130 b must have formed farther out in the disk and subsequently migrated inward due to dynamical interactions with either the primordial gaseous protoplanetary disk or other bodies.

The possibility that HD 119130 b formed farther out in the disk—perhaps beyond the snow line, where large planetary embryos are expected to grow quickly ([Kokubo & Ida 2002](#); [Morbidelli et al. 2015](#))—does not necessarily preclude a water-poor composition ([Raymond et al. 2018](#)). Measurements of the planet’s atmospheric metallicity could break the degeneracy in composition by determining if the planet has a H/He- or steam-dominated envelope. The planet’s Transmission Spectroscopy Metric (TSM; [Kempton et al. 2018](#)), a *JWST* S/N proxy, is  $\text{TSM} = 31_{-9}^{+19}$ , which corresponds to the 54th percentile of TSM values for the confirmed planets that underlie the contours in Figure 9.

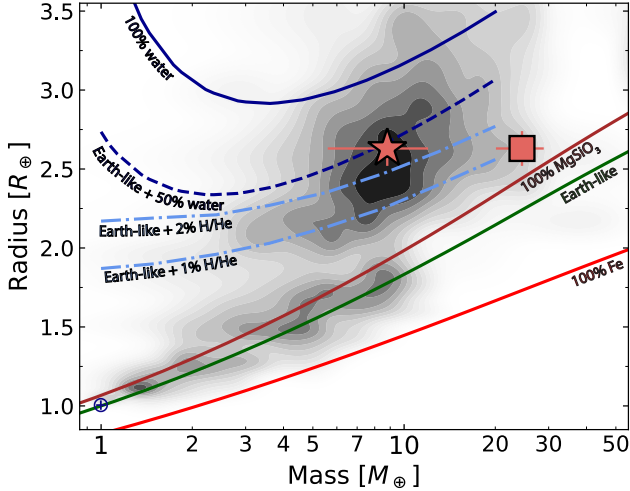


**Figure 9.** The mass-radius diagram in the sub-Neptune and super-Earth regime. Contours are computed using Gaussian kernel density estimation on the population of confirmed planets with better than 33% and 15% measurement precision on mass and radius, respectively (NASA Exoplanet Archive 2024). Composition curves are shown for reference. The two dash-dot light blue curves represent Earth-like cores surrounded by 1% and 2% by mass H/He-dominated, solar-metallicity envelopes for a planet receiving 10 times Earth’s insolation orbiting a 10 Gyr-old star (Lopez & Fortney 2014). HD 119130 b’s instellation is  $S_p = 67 S_\oplus$ . The solid red, green, and brown curves represent a pure iron, Earth-like, and pure silicate composition, respectively (Zeng et al. 2016). The dashed dark blue curve represents an irradiated “water world” at  $T_{\text{eq}} = 800$  K made of an Earth-like core and 50%  $\text{H}_2\text{O}$ , by mass, in the form of a supercritical  $\text{H}_2\text{O}$  fluid layer and a steam-dominated envelope; the solid dark blue curve represents a composition of 100% supercritical  $\text{H}_2\text{O}$  and steam at  $T_{\text{eq}} = 800$  K (Aguichine et al. 2021). HD 119130 b is shown as both the square (L19 mass measurement) and the star (this work) for comparison.

## 6. CONCLUSION

We obtained 57 new RVs of the G dwarf, HD 119130, using HARPS, HARPS-N, and HIRES. Combined with the 18 existing CARMENES RVs from L19, our follow-up observations reveal that the transiting sub-Neptune, HD 119130 b, is not unusually massive for its size, as previously thought. In fact, our mass measurement of HD 119130 b is almost three times smaller than the value from L19. The case of HD 119130 b serves as a cautionary tale for observers analyzing modestly-sized RV data sets.

Our conclusions are summarized as follows:

- HD 119130 b ( $R_p = 2.63^{+0.11}_{-0.10} R_\oplus$ ) has  $M_p = 8.8 \pm 3.2 M_\oplus$  ( $M_p < 15.4 M_\oplus$  at 98% confidence). Our mass measurement differs from the L19 value at

the  $2.9\sigma$ -level. The planet is not an “ultra-dense” sub-Neptune.

- We detect a candidate signal in the RVs at  $P \approx 200$  days with  $K = 4.9 \pm 1.2 \text{ m s}^{-1}$ . Additional RV monitoring is required to determine the signal’s true nature.
- The inaccuracy of the L19 mass measurement can be explained by the presence of an additional sinusoidal signal in the data. With  $P = 12$  days, this signal could feasibly represent either the stellar rotation period or its first harmonic.

As we begin to study small-planet demographics in the mass-radius plane (e.g., Luque & Pallé 2022), the community should endeavor to ensure that these mass measurements are both precise *and* accurate, lest they bias our understanding of the physics of planet formation.

## ACKNOWLEDGMENTS

The authors thank the anonymous reviewer for their thoughtful report, which improved the manuscript.

The authors wish to recognize and acknowledge the very significant cultural role and reverence that Maunakea has always had within the indigenous Hawaiian community. We are most fortunate to have the opportunity to conduct observations from this sacred mountain, which is now colonized land.

J.M.A.M. thanks Jacob Bean for detailed comments that improved the manuscript. J.M.A.M. thanks the Keck-HIRES observers for obtaining data of HD 119130. In order of the number of observations contributed, the observers are: Judah Van Zandt, Fei Dai, Steven Gicalone, Rae Holcomb, Howard Isaacson, Corey Beard, Samuel Yee, Lauren Weiss, Jingwen Zhang, and Luke Bouma.

J.M.A.M. is supported by the National Science Foundation (NSF) Graduate Research Fellowship Program (GRFP) under Grant No. DGE-1842400. J.M.A.M. and N.M.B. acknowledge support from NASA’S Interdisciplinary Consortia for Astrobiology Research (NNH19ZDA001N-ICAR) under award number 19-ICAR19.2-0041.

V.V.E. is supported by UK’s Science & Technology Facilities Council (STFC) through the STFC grants ST/W001136/1 and ST/S000216/1.

Support for this work was provided by NASA through the NASA Hubble Fellowship grant #HF2-51559 awarded by the Space Telescope Science Institute, which is operated by the Association of Universities for

Research in Astronomy, Inc., for NASA, under contract NAS5-26555.

This work used **Expanse** at the San Diego Supercomputer Center through allocation PHY220015 from the Advanced Cyberinfrastructure Coordination Ecosystem: Services & Support (ACCESS) program, which is supported by NSF grants 2138259, 2138286, 2138307, 2137603, and 2138296.

Some of the data presented herein were obtained at Keck Observatory, which is a private 501(c)3 non-profit organization operated as a scientific partnership among the California Institute of Technology, the University of California, and the National Aeronautics and Space Administration. The Observatory was made possible by the generous financial support of the W. M. Keck Foundation.

We acknowledge financial support from the Agencia Estatal de Investigación of the Ministerio de Ciencia e Innovación MCIN/AEI/10.13039/501100011033 and the ERDF “A way of making Europe” through project PID2021-125627OB-C32, and from the Centre of Excellence “Severo Ochoa” award to the Instituto de Astrofísica de Canarias.

G.N. acknowledges financial support from the Ministry of Science and Higher Education program the “Excellence Initiative - Research University” conducted at the Centre of Excellence in Astrophysics and Astrochemistry of the Nicolaus Copernicus University in Toruń, Poland. G.N. gratefully acknowledges the Centre of Informatics Tricity Academic Supercomputer and network (CI TASK, Gdańsk, Poland) for computing resources (grant no. PT01016).

This work benefited from the 2023 Exoplanet Summer Program in the Other Worlds Laboratory (OWL) at the University of California, Santa Cruz, a program funded by the Heising-Simons Foundation.

*Facilities:* HARPS, HARPS-N, Keck:I (HIRES).

*Software:* **exoplanet** (Foreman-Mackey et al. 2020), **matplotlib** (Hunter 2007), **numpy** (Harris et al. 2020), **pandas** (pandas development team 2020), Python 3 (Van Rossum & Drake 2009), **RadVel** (Fulton et al. 2018), **RVSearch** (Rosenthal et al. 2021).

## REFERENCES

- Aguichine, A., Mousis, O., Deleuil, M., & Marcq, E. 2021, *ApJ*, 914, 84, doi: [10.3847/1538-4357/abfa99](https://doi.org/10.3847/1538-4357/abfa99)
- Akaike, H. 1974, *IEEE Transactions on Automatic Control*, 19, 716
- Akana Murphy, J. M., Luque, R., & Batalha, N. M. 2024, arXiv e-prints, arXiv:2411.02521, doi: [10.48550/arXiv.2411.02521](https://doi.org/10.48550/arXiv.2411.02521)
- Akana Murphy, J. M., Kosiarek, M. R., Batalha, N. M., et al. 2021, *AJ*, 162, 294, doi: [10.3847/1538-3881/ac2830](https://doi.org/10.3847/1538-3881/ac2830)
- Armstrong, D. J., Lopez, T. A., Adibekyan, V., et al. 2020, *Nature*, 583, 39, doi: [10.1038/s41586-020-2421-7](https://doi.org/10.1038/s41586-020-2421-7)
- Baluev, R. V. 2008, *MNRAS*, 385, 1279, doi: [10.1111/j.1365-2966.2008.12689.x](https://doi.org/10.1111/j.1365-2966.2008.12689.x)
- Betancourt, M., & Girolami, M. 2015, *Current trends in Bayesian methodology with applications*, 79, 2. <https://arxiv.org/abs/1312.0906>
- Blunt, S., Carvalho, A., David, T. J., et al. 2023, *AJ*, 166, 62, doi: [10.3847/1538-3881/acde78](https://doi.org/10.3847/1538-3881/acde78)
- Burnham, K. P., & Anderson, D. R. 2002, *Model Selection and Multimodel Inference* (Springer-Verlag New York)
- Burnham, K. P., & Anderson, D. R. 2004, *Sociological Methods & Research*, 33, 261, doi: [10.1177/0049124104268644](https://doi.org/10.1177/0049124104268644)
- Burt, J., Holden, B., Wolfgang, A., & Bouma, L. G. 2018, *AJ*, 156, 255, doi: [10.3847/1538-3881/aae697](https://doi.org/10.3847/1538-3881/aae697)
- Butler, R. P., Marcy, G. W., Williams, E., et al. 1996, *Publications of the Astronomical Society of the Pacific*, 108, 500, doi: [10.1086/133755](https://doi.org/10.1086/133755)
- Cosentino, R., Lovis, C., Pepe, F., et al. 2012, in *Society of Photo-Optical Instrumentation Engineers (SPIE) Conference Series*, Vol. 8446, *Ground-based and Airborne Instrumentation for Astronomy IV*, ed. I. S. McLean, S. K. Ramsay, & H. Takami, 84461V, doi: [10.1117/12.925738](https://doi.org/10.1117/12.925738)
- Cosentino, R., Lovis, C., Pepe, F., et al. 2014, in *Society of Photo-Optical Instrumentation Engineers (SPIE) Conference Series*, Vol. 9147, *Ground-based and Airborne Instrumentation for Astronomy V*, ed. S. K. Ramsay, I. S. McLean, & H. Takami, 91478C, doi: [10.1117/12.2055813](https://doi.org/10.1117/12.2055813)
- Dawson, R. I., & Chiang, E. 2014, *Science*, 346, 212, doi: [10.1126/science.1256943](https://doi.org/10.1126/science.1256943)
- Dragomir, D., Teske, J., Günther, M. N., et al. 2019, *ApJL*, 875, L7, doi: [10.3847/2041-8213/ab12ed](https://doi.org/10.3847/2041-8213/ab12ed)
- Duane, S., Kennedy, A. D., Pendleton, B. J., & Roweth, D. 1987, *Physics Letters B*, 195, 216, doi: [10.1016/0370-2693\(87\)91197-X](https://doi.org/10.1016/0370-2693(87)91197-X)
- Eastman, J., Siverd, R., & Gaudi, B. S. 2010, *PASP*, 122, 935, doi: [10.1086/655938](https://doi.org/10.1086/655938)

- Foreman-Mackey, D., Luger, R., Czekala, I., et al. 2020, *exoplanet-dev/exoplanet* v0.3.2, doi: [10.5281/zenodo.1998447](https://doi.org/10.5281/zenodo.1998447)
- Fulton, B. J., Petigura, E. A., Blunt, S., & Sinukoff, E. 2018, *PASP*, 130, 044504, doi: [10.1088/1538-3873/aaa8](https://doi.org/10.1088/1538-3873/aaa8)
- Gaia Collaboration, Prusti, T., de Bruijne, J. H. J., et al. 2016, *A&A*, 595, A1, doi: [10.1051/0004-6361/201629272](https://doi.org/10.1051/0004-6361/201629272)
- Gaia Collaboration, Vallenari, A., Brown, A. G. A., et al. 2023, *A&A*, 674, A1, doi: [10.1051/0004-6361/202243940](https://doi.org/10.1051/0004-6361/202243940)
- Gan, T., Wang, S. X., Teske, J. K., et al. 2021, *MNRAS*, 501, 6042, doi: [10.1093/mnras/staa3886](https://doi.org/10.1093/mnras/staa3886)
- Gelman, A., & Rubin, D. B. 1992, *Statistical Science*, 7, 457, doi: [10.1214/ss/1177011136](https://doi.org/10.1214/ss/1177011136)
- Grunblatt, S. K., Howard, A. W., & Haywood, R. D. 2015, *ApJ*, 808, 127, doi: [10.1088/0004-637X/808/2/127](https://doi.org/10.1088/0004-637X/808/2/127)
- Guerrero, N. M., Seager, S., Huang, C. X., et al. 2021, *ApJS*, 254, 39, doi: [10.3847/1538-4365/abef1](https://doi.org/10.3847/1538-4365/abef1)
- Hadden, S., & Lithwick, Y. 2014, *ApJ*, 787, 80, doi: [10.1088/0004-637X/787/1/80](https://doi.org/10.1088/0004-637X/787/1/80)
- Harris, C. R., Millman, K. J., van der Walt, S. J., et al. 2020, *Nature*, 585, 357, doi: [10.1038/s41586-020-2649-2](https://doi.org/10.1038/s41586-020-2649-2)
- Hoffman, M., & Gelman, A. 2014, *J. Mach. Learn. Res.*, 15, 1593
- Horne, J. H., & Baliunas, S. L. 1986, *ApJ*, 302, 757, doi: [10.1086/164037](https://doi.org/10.1086/164037)
- Houk, N., & Swift, C. 1999, *Michigan Spectral Survey*, 5, 0
- Howard, A. W., & Fulton, B. J. 2016, *Publications of the Astronomical Society of the Pacific*, 128, 114401, doi: [10.1088/1538-3873/128/969/114401](https://doi.org/10.1088/1538-3873/128/969/114401)
- Howard, A. W., Johnson, J. A., Marcy, G. W., et al. 2010, *The Astrophysical Journal*, 721, 1467, doi: [10.1088/0004-637x/721/2/1467](https://doi.org/10.1088/0004-637x/721/2/1467)
- Howell, S. B., Sobek, C., Haas, M., et al. 2014, *Publications of the Astronomical Society of the Pacific*, 126, 398
- Huber, D., Bryson, S. T., Haas, M. R., et al. 2016, *ApJS*, 224, 2, doi: [10.3847/0067-0049/224/1/2](https://doi.org/10.3847/0067-0049/224/1/2)
- Hunter, J. D. 2007, *Computing in Science & Engineering*, 9, 90, doi: [10.1109/MCSE.2007.55](https://doi.org/10.1109/MCSE.2007.55)
- Isaacson, H., Howard, A. W., Fulton, B., et al. 2024, *ApJS*, 274, 35, doi: [10.3847/1538-4365/ad676c](https://doi.org/10.3847/1538-4365/ad676c)
- Jontof-Hutter, D. 2019, *Annual Review of Earth and Planetary Sciences*, 47, 141, doi: [10.1146/annurev-earth-053018-060352](https://doi.org/10.1146/annurev-earth-053018-060352)
- Kempton, E. M. R., Bean, J. L., Louie, D. R., et al. 2018, *PASP*, 130, 114401, doi: [10.1088/1538-3873/aad6f](https://doi.org/10.1088/1538-3873/aad6f)
- Kennedy, G. M., & Kenyon, S. J. 2008, *ApJ*, 673, 502, doi: [10.1086/524130](https://doi.org/10.1086/524130)
- Kokubo, E., & Ida, S. 2002, *ApJ*, 581, 666, doi: [10.1086/344105](https://doi.org/10.1086/344105)
- Kosiarek, M. R., Berardo, D. A., Crossfield, I. J. M., et al. 2021, *AJ*, 161, 47, doi: [10.3847/1538-3881/abca39](https://doi.org/10.3847/1538-3881/abca39)
- Kovács, G., Zucker, S., & Mazeh, T. 2002, *A&A*, 391, 369, doi: [10.1051/0004-6361:20020802](https://doi.org/10.1051/0004-6361:20020802)
- Lacedelli, G., Pallè, E., Luque, R., et al. 2024, arXiv e-prints, arXiv:2409.11083, doi: [10.48550/arXiv.2409.11083](https://doi.org/10.48550/arXiv.2409.11083)
- Lange, S., Murphy, J. M. A., Batalha, N. M., et al. 2024, *The Astronomical Journal*, 167, 282, doi: [10.3847/1538-3881/ad34d9](https://doi.org/10.3847/1538-3881/ad34d9)
- Lecavelier Des Etangs, A. 2007, *A&A*, 461, 1185, doi: [10.1051/0004-6361:20065014](https://doi.org/10.1051/0004-6361:20065014)
- Lee, E. J., & Chiang, E. 2016, *ApJ*, 817, 90, doi: [10.3847/0004-637X/817/2/90](https://doi.org/10.3847/0004-637X/817/2/90)
- Libby-Roberts, J. E., Berta-Thompson, Z. K., Désert, J.-M., et al. 2020, *AJ*, 159, 57, doi: [10.3847/1538-3881/ab5d36](https://doi.org/10.3847/1538-3881/ab5d36)
- Lomb, N. R. 1976, *Ap&SS*, 39, 447, doi: [10.1007/BF00648343](https://doi.org/10.1007/BF00648343)
- Lopez, E. D., & Fortney, J. J. 2014, *ApJ*, 792, 1, doi: [10.1088/0004-637X/792/1/1](https://doi.org/10.1088/0004-637X/792/1/1)
- Luger, R., Kruse, E., Foreman-Mackey, D., Agol, E., & Saunders, N. 2018, *AJ*, 156, 99, doi: [10.3847/1538-3881/aad230](https://doi.org/10.3847/1538-3881/aad230)
- Lundkvist, M. S., Kjeldsen, H., Albrecht, S., et al. 2016, *Nature Communications*, 7, 11201, doi: [10.1038/ncomms11201](https://doi.org/10.1038/ncomms11201)
- Luque, R., & Pallé, E. 2022, *Science*, 377, 1211, doi: [10.1126/science.abl7164](https://doi.org/10.1126/science.abl7164)
- Luque, R., Nowak, G., Pallé, E., et al. 2019, *A&A*, 623, A114, doi: [10.1051/0004-6361/201834952](https://doi.org/10.1051/0004-6361/201834952)
- Mayor, M., Pepe, F., Queloz, D., et al. 2003, *The Messenger*, 114, 20
- Morbidelli, A., Lambrechts, M., Jacobson, S., & Bitsch, B. 2015, *Icarus*, 258, 418, doi: [10.1016/j.icarus.2015.06.003](https://doi.org/10.1016/j.icarus.2015.06.003)
- Munari, U., Henden, A., Frigo, A., et al. 2014, *AJ*, 148, 81, doi: [10.1088/0004-6256/148/5/81](https://doi.org/10.1088/0004-6256/148/5/81)
- Mustill, A. J., Davies, M. B., & Johansen, A. 2017, *MNRAS*, 468, 3000, doi: [10.1093/mnras/stx693](https://doi.org/10.1093/mnras/stx693)
- NASA Exoplanet Archive. 2024, *Planetary Systems*, Version: 2024-09-02 17:46, NExSci-Caltech/IPAC, doi: [10.26133/NEA12](https://doi.org/10.26133/NEA12)
- Neal, R. M. 2003, *The Annals of Statistics*, 31, 705–767, doi: [10.1214/aos/1056562461](https://doi.org/10.1214/aos/1056562461)
- Neal, R. M. 2012, arXiv e-prints, arXiv:1206.1901. <https://arxiv.org/abs/1206.1901>
- Owen, J. E., & Wu, Y. 2013, *ApJ*, 775, 105, doi: [10.1088/0004-637X/775/2/105](https://doi.org/10.1088/0004-637X/775/2/105)
- pandas development team, T. 2020, *pandas-dev/pandas: Pandas, latest*, Zenodo, doi: [10.5281/zenodo.3509134](https://doi.org/10.5281/zenodo.3509134)

- Petigura, E. A., Howard, A. W., Marcy, G. W., et al. 2017, *The Astronomical Journal*, 154, 107, doi: [10.3847/1538-3881/aa80de](https://doi.org/10.3847/1538-3881/aa80de)
- Quirrenbach, A., Amado, P. J., Caballero, J. A., et al. 2014, in *Society of Photo-Optical Instrumentation Engineers (SPIE) Conference Series*, Vol. 9147, *Ground-based and Airborne Instrumentation for Astronomy V*, ed. S. K. Ramsay, I. S. McLean, & H. Takami, 91471F, doi: [10.1117/12.2056453](https://doi.org/10.1117/12.2056453)
- Quirrenbach, A., Amado, P. J., Ribas, I., et al. 2018, in *Society of Photo-Optical Instrumentation Engineers (SPIE) Conference Series*, Vol. 10702, *Ground-based and Airborne Instrumentation for Astronomy VII*, ed. C. J. Evans, L. Simard, & H. Takami, 107020W, doi: [10.1117/12.2313689](https://doi.org/10.1117/12.2313689)
- Rajpaul, V., Buchhave, L. A., & Aigrain, S. 2017, *MNRAS*, 471, L125, doi: [10.1093/mnras/slx116](https://doi.org/10.1093/mnras/slx116)
- Rasmussen, C. E., & Williams, C. K. I. 2006, *Gaussian Processes for Machine Learning* (MIT Press)
- Raymond, S. N., Boulet, T., Izidoro, A., Esteves, L., & Bitsch, B. 2018, *MNRAS*, 479, L81, doi: [10.1093/mnras/sly100](https://doi.org/10.1093/mnras/sly100)
- Ricker, G. R., Winn, J. N., Vanderspek, R., et al. 2014, *Journal of Astronomical Telescopes, Instruments, and Systems*, 1, 1, doi: [10.1117/1.JATIS.1.1.014003](https://doi.org/10.1117/1.JATIS.1.1.014003)
- Rosenthal, L. J., Fulton, B. J., Hirsch, L. A., et al. 2021, *ApJS*, 255, 8, doi: [10.3847/1538-4365/abe23c](https://doi.org/10.3847/1538-4365/abe23c)
- Salvatier, J., Wiecki, T. V., & Fonnesbeck, C. 2016, *PeerJ Computer Science*, 2, doi: [10.7717/peerj-cs.55](https://doi.org/10.7717/peerj-cs.55)
- Savitzky, A., & Golay, M. J. E. 1964, *Analytical Chemistry*, 36, 1627
- Scargle, J. D. 1982, *ApJ*, 263, 835, doi: [10.1086/160554](https://doi.org/10.1086/160554)
- Schlichting, H. E. 2014, *ApJL*, 795, L15, doi: [10.1088/2041-8205/795/1/L15](https://doi.org/10.1088/2041-8205/795/1/L15)
- Schwarz, G. 1978, *Annals of Statistics*, 6, 461
- Sinukoff, E., Howard, A. W., Petigura, E. A., et al. 2017, *AJ*, 153, 271, doi: [10.3847/1538-3881/aa725f](https://doi.org/10.3847/1538-3881/aa725f)
- Skrutskie, M. F., Cutri, R. M., Stiening, R., et al. 2006, *AJ*, 131, 1163, doi: [10.1086/498708](https://doi.org/10.1086/498708)
- Southworth, J. 2011, *MNRAS*, 417, 2166, doi: [10.1111/j.1365-2966.2011.19399.x](https://doi.org/10.1111/j.1365-2966.2011.19399.x)
- Szabó, G. M., & Kiss, L. L. 2011, *ApJL*, 727, L44, doi: [10.1088/2041-8205/727/2/L44](https://doi.org/10.1088/2041-8205/727/2/L44)
- Van Rossum, G., & Drake, F. L. 2009, *Python 3 Reference Manual* (Scotts Valley, CA: CreateSpace)
- Vanderburg, A., Plavchan, P., Johnson, J. A., et al. 2016, *MNRAS*, 459, 3565, doi: [10.1093/mnras/stw863](https://doi.org/10.1093/mnras/stw863)
- Vehtari, A., Gelman, A., Simpson, D., Carpenter, B., & Bürkner, P.-C. 2021, *Bayesian Analysis*, 16, 667, doi: [10.1214/20-BA1221](https://doi.org/10.1214/20-BA1221)
- Vogt, S. S., Allen, S. L., Bigelow, B. C., et al. 1994, in *Society of Photo-Optical Instrumentation Engineers (SPIE) Conference Series*, Vol. 2198, *Instrumentation in Astronomy VIII*, ed. D. L. Crawford & E. R. Craine, 362, doi: [10.1117/12.176725](https://doi.org/10.1117/12.176725)
- Zechmeister, M., & Kürster, M. 2009, *A&A*, 496, 577, doi: [10.1051/0004-6361:200811296](https://doi.org/10.1051/0004-6361:200811296)
- Zeng, L., Sasselov, D. D., & Jacobsen, S. B. 2016, *ApJ*, 819, 127, doi: [10.3847/0004-637X/819/2/127](https://doi.org/10.3847/0004-637X/819/2/127)